GEOCHRONOLOGY
Discussions
Open Access
EGU

An optimization tool for identifying Multiple Diffusion Domain Model parameters

Andrew L. Gorin[1,2], Joshua M. Gorin[3], Marie Bergelin[2], and David L. Shuster[1,2]

[1]Department of Earth and Planetary Science, University of California, Berkeley, CA
[2]Berkeley Geochronology Center, Berkeley, CA
[3]Independent Researcher

Correspondence: Andrew Gorin (andrew_gorin@berkeley.edu)

Abstract. The Multiple-Diffusion Domain (MDD) model empirically describes the diffusive behavior of noble gases in some terrestrial materials and has been commonly used to interpret $^{40}Ar/^{39}Ar$ stepwise degassing observations in K-feldspar. When applied in this manner, the MDD model can be used to test crustal exhumation scenarios by identifying the permissible thermal paths a rock sample could have undergone over geological time, assuming the diffusive properties of Ar within the mineral are accurately understood. More generally, the MDD model provides a framework for quantifying the temperature-dependent
5   diffusivity of noble gasses in minerals. However, constraining MDD parameters that successfully predict the results of step-heating diffusion experiments is a complex task and the assumptions made by existing numerical methods used to quantify model parameters can bias the absolute temperatures permitted by thermal modeling. For example, the most commonly used method (Lovera et al., 1997) assumes that no domains lose more than 60% of their gas during early heating steps. This assump-
10   tion is unverifiable, and we show that Lovera et al.'s (1997) procedure may bias predicted temperatures towards lower values when it is violated. To address this potential bias and to provide greater accessibility to the MDD model, we present a new, open-source method for constraining MDD parameters from stepwise degassing experimental results, called the "MDD Tool Kit." This software optimizes all MDD parameters simultaneously and removes any need for user-defined E_a or regression-fitting choices used by other tools. In doing so, this new method eliminates assumptions about the domain size distribution.
15   To test the validity of our thermal predictions, we then use the MDD Tool Kit to interpret the $^{40}Ar/^{39}Ar$ results of Wong et al. (2023) from the Grayback Fault, AZ, USA. Although the resulting thermal histories are consistently $\sim 60 - 75$ °C higher than those found by Wong et al. (2023), they agree with independent observations from apatite fission track, zircon fission track, and (U-Th)/He (Howard and Foster, 1996).

1   Introduction

20   $^{40}Ar/^{39}Ar$ thermochronology is a valuable tool for studying Earth's crustal exhumation because it constrains a mineral's continuous thermal history through geologic time (McDougall and Harrison, 1999). While $^{40}Ar/^{39}Ar$ geochronology was initially developed to quantify crystallization timing of rapidly-cooled igneous rocks (Turner, 1968), its application to thermochronology did not begin in earnest until Dodson's (1973) quantitative description of closure theory, which allowed one to determine when a mineral cooled below a mineral-specific "closure temperature" for radiogenic ^{40}Ar retention (Reiners, 2005). Dur-

25 ing this early period of thermochronology research, minerals and isotopic systems with disparate closure temperatures were combined to constrain a given rock's permissible thermal histories (e.g. Wagner, 1977). While this approach yielded valuable insight into Earth's surface processes (McDougall and Harrison, 1999), it requires that multiple mineral phases—which are always present—to coexist in a sample. Further, the thermal histories inferred from this technique are discontinuous, with one age-temperature measurement for each mineral phase, thus limiting the ability to quantify cooling rates at specific times

30 (McDougall and Harrison, 1999), and potentially introducing biases. Additionally, this approach does not fully accommodate the complexity of the diffusive properties observed in some minerals (Zeitler, 1987; McDougall and Harrison, 1999).

Since the late 1960s, it had been understood that complex retention properties pose challenges for interpreting the thermal histories of some samples. More specifically, the results of some stepwise degassing experiments were not consistent with volume diffusion from a single domain in some minerals, requiring a new interpretative framework (Zeitler, 1987; Lovera

35 et al., 1989). Progress came first with Zeitler's (1987) observations in K-feldspar that the anomalous behavior seen in their ^{40}Ar/^{39}Ar age spectra and associated Arrhenius plots could be explained by outward diffusion of ^{39}Ar from several "domains" (distinct, non-interacting geometries in which volume diffusion takes place) of varying sizes simultaneously. A formalism for this model, called the Multiple-Diffusion Domain (MDD) Model, was then described by Lovera et al (1989). This model enabled more nuanced interpretations of sample-specific diffusion kinetics—and thereby thermal histories—of minerals.

40 While this model has received criticism (e.g. Villa, 1994; Parsons et al., 1999), it has largely been adopted by the thermochronology community since the 2000s due to its ability to constrain time-temperature (t-T) histories that are consistent with both an observed ^{40}Ar/^{39}Ar age spectrum and calculated diffusion kinetics of a given sample (Reiners, 2005; Harrison and Lovera, 2014). However, we show that the method used by Lovera et al. (1997) to tune the MDD model parameters to match the results of a step-heating diffusion experiment potentially introduces a systematic bias towards colder temperatures through

45 geologic time. This was recognized, but not addressed, at the time of their publication, likely due to insufficient computing power to resolve the issue (Lovera et al., 1997).

2 The MDD Model

The MDD model is best understood through analogy to volume diffusion through a single domain. In this simple case, the temperature-dependent diffusivity is described by

50 $$\frac{D(T)}{a^2} = \frac{D_0}{a^2} * e^{\frac{-E_a}{RT}} \tag{1}$$

where T is the absolute temperature (K), D is diffusivity at T in (cm$^2\cdot$ sec^{-1}), D_0 is diffusivity at infinite T, E_a is activation energy (kJ·mol^{-1}), R is the gas constant (kJ·mol^{-1}·K^{-1}), and a is the radius of the diffusion domain (cm).

This relationship is typically determined empirically for noble gas diffusion in minerals through a stepwise degassing diffusion experiment. In such experiments, the diffusant is first produced in-situ by a proton or neutron irradiation to ensure a

55 homogeneous initial distribution. The sample is then placed under static vacuum where it is repeatedly heated to a known temperature, and the quantity of the diffusant is measured (Fechtig and Kalbitzer, 1966; McDougall and Harrison, 1999). By

assuming a geometry for the diffusion domain, the fractional loss at each step can be used to calculate a corresponding $\frac{D}{a^2}$ with the equations of Fechtig and Kalbitzer (1966) or Crank (1975). Ginster and Reiners (2018) summarized and propagated measurement uncertainties through these equations and we use their forms in this work (Table 1).

60   When consistent with volume diffusion through a single diffusion domain, a step-heating experiment will produce a linear Arrhenius relationship between calculated values of $\log(\frac{D}{a^2})$ and $\frac{1}{T}$. In these cases, a linear regression can then be fit to the results to determine E_a and $\frac{D_0}{a_0^2}$ (Lovera et al., 1997) for a sample. Several mineral-diffusant pairs such as ^{3}He in apatite and ^{3}He in olivine exhibit such behavior (Shuster et al., 2004).

However, not all minerals exhibit diffusive behavior consistent with volume diffusion from a single diffusion domain. The
65   diffusive behavior of some minerals appears to be more consistent with diffusion from several, non-interacting domains of varying sizes, within a given mineral, diffusing simultaneously. This behavior was later identified and roughly quantified by Gillespie et al. (1982) and Zeitler (1987) in K-feldspar, orthoclase, and microcline, and then formalized by Lovera et al. (1989).

In contrast to the single diffusion domain model, the MDD model can be imagined as a series of non-interacting diffusion domains of varying diffusive length scale (e.g., different radii, a) that all diffuse simultaneously. The choice of geometry
70   for the domains is somewhat arbitrary, as it remains unclear what these diffusion domains physically represent in a mineral sample (Harrison and Lovera, 2014). Some authors use a plane sheet, while others prefer a spherical or cylindrical geometry. Regardless of this choice, it is assumed that each diffusion domain has the same geometry, E_a, and D_0. Therefore, a diffusion domain can be described completely by three parameters: (i) E_a (common to all domains), (ii) its pre-exponential term $(\frac{D_0}{a^2})_i$ and (iii) the proportion of the total gas it contains (ϕ). Thus, a multiple-diffusion domain model with n domains has $2n-1$ free
75   parameters because $\sum_{i=1}^{n} \phi_n = 1$.

An inherent challenge in applying this model is that each of these $2n-1$ parameters need to be optimized to accurately predict the results of a given diffusion experiment. Because authors using the MDD model fit as many as 10 domains, this optimization is regularly performed on 19-dimensional vectors or larger, making the exercise non-trivial.

3   Existing Optimization Methods

80   The Lovera et al. (1997) method for identifying MDD model parameters is the only published algorithm for this purpose that we are aware of and has been used in many studies (e.g. Harrison et al., 1995; Quidelleur et al., 1997; Grove et al., 2003; Weirich et al., 2012; Wong et al., 2023). The routine begins by defining a reference domain which is used to calculate an E_a by fitting an uncertainty-weighted linear regression to the $\log_{10}(\frac{D}{a^2})$ values resulting from a subset of the low temperature heating steps in an Arrhenius plot; the resultant E_a is assumed applicable to all domains. This is done because—even in samples
85   exhibiting MDD-like behavior—these diffusivities tend to approximate a line (Figure 1A).

To determine the number of points to include in the uncertainty-weighted linear regression, the lowest temperature heating steps are sequentially added to the regression. After adding each step, a chi-squared misfit static is calculated and is then used to calculate a goodness-of-fit probability (q) (Lovera et al., 1997). These relationships are described as follows:

$$\chi^2_{lovera} = \sum_{i=1}^{N} \left(\frac{\log_{10}(\frac{D}{a^2})_i - \log_{10}(\frac{\hat{D}}{a^2})_i}{\sigma_i} \right)^2 \tag{2}$$

90

$$q = \mathrm{gammq}\left(\frac{N-2}{2}, \frac{\chi^2}{2} \right) \tag{3}$$

where $gammq$ is the incomplete gamma function, $(\frac{D}{a^2})_i$ is the observed pre-exponential term, $(\frac{\hat{D}}{a^2})_i$ is the modeled pre-exponential term, σ is the uncertainty on the observed pre-exponential term, and N is the number of steps included (Lovera et al., 1997; Press, 2007). This calculation is repeated until the value of $q \cdot N$ is maximized. Once the E_a is determined from

95 the above process, this value is held fixed while a Levenberg-Marquardt method (Press, 2007) is used to adjust the gas fraction (ϕ) and $\log_{10}(\frac{D_0}{a^2})$ for each domain to minimize the above chi-square quantity. The reader is directed to Appendix B of Lovera et al. (1997) and the referenced sections of Press (2007) for additional information.

While this routine is generally robust and capable of accurately quantifying E_a in synthetic data experiments where the kinetics are defined, it fails to do so when the smallest domains lose greater than 60% of their gas in early heating steps (Figure

100 1). Thus, use of this routine makes the implicit assumption that no domains diffuse most of their gas during the initial heating steps. When this assumption is violated, the regression will overestimate the E_a and $\log_{10}(\frac{D_0}{a_0^2})$ (Figure 1). Because there is currently no way to know the domain size distribution *a priori*, it is not possible to know whether this assumption is valid for any given sample (Lovera et al., 1997).

Furthermore, Lovera et al. (1997) found evidence that the variability of predicted E_a values from different aliquots of the

105 same mineral decreased when they were able to use a higher percentage of the total gas released in their linear regressions. Simply put, the more gas included in the calculation, the less variation there was in predicted E_a. This observation suggests that a routine which maximizes the fraction of ^{39}Ar used in the fitting exercise might lead to more precise estimates of diffusion kinetics.

4 The MDD Tool Kit Approach

110 With the increased computational power since the publication of the original routine for optimizing these models, we apply SciPy's implementation of the differential evolution algorithm to fit all the diffusion kinetics parameters simultaneously (Storn and Price, 1997; Lampinen, 2002; Qiang and Mitchell, 2014; Virtanen et al., 2020). This algorithm is a population-based genetic algorithm for optimizing over continuous search spaces in high dimensions with non-linear and non-differentiable misfit functions (Storn and Price, 1997).

4.1 Differential Evolution

115

Our implementation of SciPy's differential evolution is a method for iteratively improving a randomly selected "population" of guesses until the best-fitting diffusion kinetics are found (Figure 2). The algorithm improves these guesses by combining

elements of the most successful vectors with those remaining. In this case, success refers to the value of a misfit statistic calculated between the guess's forward-modeled gas releases and the observed results. Through this process, each successive

120   generation achieves a misfit equal to or lower than the previous one.

We apply two such misfit statistics to the data analyzed in this study, one error weighted, χ^2, and another where all points are weighted equally ($\%_{frac}$). Our χ^2 misfit accounts for the uncertainty on the ^{39}Ar measurements by performing its calculations in units of moles so that the measurement uncertainty can readily be included. This is accomplished by multiplying the forward-modeled gas fractions (F_i) by the total number of moles released during the experiment. Because this value is not directly

125   measured, we add it as a parameter to our model ($\hat{M}_{tot}$) and allow our optimization algorithm to solve for it when using this misfit statistic. We allow the model allowed to choose any $\hat{M}_{tot}$ value within 3σ of the observed value. Our χ^2 misfit statistic is thereby defined as follows:

$$\chi^2 = \sum_{i=1}^{N} \left(\frac{M_i - \hat{F}_i \hat{M}_{tot}}{\sigma_i}\right)^2 \tag{4}$$

By contrast, $\%_{frac}$ weights all heating steps equally, regardless of their associated measurement uncertainty. This misfit reports

130   a percent difference between the measured and modeled gas fraction released at each step and is defined as follows:

$$\%_{Frac} = \sum_{i=1}^{N} \frac{F_i - \hat{F}_i}{F_i} \tag{5}$$

where F_i is the measured gas fraction at a given heating step, and $\hat{F}_i$ is the modeled gas fraction at a given heating step.

Regardless of which misfit statistic is used, differential evolution optimizes the parameters in the same way, and begins by generating its initial population. Given a vector of parameters to be tuned for an n-domain model,

135    $\boldsymbol{X}(\hat{M}_{tot}, E_a, \frac{D_0}{a^2}_{(i,i+1,...,n)}, \phi_{(i,i+1,...,n-1)})$, an initial population of candidate vectors is quasi-randomly generated using the Latin Hypercube method (Iman et al., 1981). These vectors ideally capture the full range of the sample space. To avoid user bias, we prescribe search ranges much larger than we imagine realistic for each variable based on prior work (Table 2; Lovera et al., 1997). Lovera et al. (1997).

From here, the improvement process is iterative. To begin, a target vector, $\boldsymbol{X}_i$, which is to be potentially improved, is

140   selected. Next, a multi-step process attempts to replace $\boldsymbol{X}_i$ with an improved offspring vector, $\boldsymbol{X}'_i$, as defined by the misfit function, g. First, the best-fit vector (i.e. lowest value of $g(\boldsymbol{X}_i)$) in the current population is copied and modified by adding a scaled value of the difference between two other randomly selected vectors in the population ($\boldsymbol{X}_{r_1}$ and $\boldsymbol{X}_{r_2}$) as follows:

$$\boldsymbol{U}_i = \boldsymbol{X}_{best} + \beta(\boldsymbol{X}_{r_1} - \boldsymbol{X}_{r_2}) \tag{6}$$

Here, β is a uniformly random value between 0.5 and 1.0. Next, $\boldsymbol{U}_i$ is combined with $\boldsymbol{X}_{best}$ to produce the offspring vector

145    $\boldsymbol{X}'_i$. This combination is performed by, for each element of $\boldsymbol{U}_i$, sampling a uniform distribution on [0,1] and replacing the element of $\boldsymbol{X}_i$ with the corresponding element of $\boldsymbol{U}_i$ if the value is less than 0.7. In this roundabout way, the trial vector's generation is informed by the existing population.

At this point, $\boldsymbol{X}_i$ has been generated, and if $g(\boldsymbol{X}'_i) < g(\boldsymbol{X}_i)$, $\boldsymbol{X}_i$ is replaced with $\boldsymbol{X}'_i$ in the population. Once the above improvement steps have been performed for every vector in the population, we advance a generation, and population metrics

150   are calculated. Based on the results of these metrics, either another generation is calculated, or the algorithm returns the best-fit vector from the population.

5   Synthetic Data Experiments

Synthetic, step-heating diffusion experiments allow for the validation of optimization methods like those described above. For a given set of diffusion kinetics parameters, one can calculate the expected amount of moles released at each step, and these

155   release fractions can then be used as an input to the optimization algorithm to search for the known diffusion kinetics parameters. If the correct parameters are returned, the optimization algorithm is validated. To evaluate the ability of our differential evolution routine (Storn and Price, 1997) in comparison to existing methods (Lovera, 1992; Lovera et al., 1997), we present the results of two such synthetic data experiments (Figure 1).

5.1   Synthetic Data Methods

160   In calculating the number of moles released for each step of a given heating schedule, two assumptions were made. First, E_a was assumed common to all domains (Lovera et al., 1997). Second, we required that the $\ln(\frac{D_0}{a^2})_i$ values of all domains differed by at least 0.25 natural log units. For the purposes of this experiment, any two domains with $\ln(\frac{D_0}{a^2})_i$ values differing by less than 0.25 were considered to be well represented by a model with one fewer domain.

   To guide our choices for the synthetic heating schedule and prescribed diffusion kinetics parameters, we used existing

165   literature on K-feldspar diffusion experiments (e.g. Lovera et al., 1997). We begin by defining Experiment A where the heating schedule and M_{tot} were selected from Lovera et al.'s (1997) N13 K-feldspar experiment because this experiment has been published many times (e.g. Lovera et al., 1997; Harrison and Lovera, 2014; Reiners et al., 2017), and because it represents a typical K-feldspar diffusion experiment. E_a was prescribed by randomly sampling from a gaussian distribution with a mean of 192.5 kJ·mol^{-1} and a σ of 25, mirroring Lovera et al.'s (1997) database of K-feldspar E_a values. The $\ln(\frac{D_0}{a^2})_i$ values were

170   selected uniformly randomly from a range of 5-25 natural log units. Finally, the ϕ_i values were prescribed randomly, requiring only that the sum of the gas fractions equal 1. The largest of these ϕ_i values were intentionally placed in the largest domains, reflecting common K-feldspar behavior.

   Experiment B was then designed to intentionally violate the assumption made by Lovera et al.'s (1997) fitting algorithm that no domain should significantly degas during early heating steps. This was done by taking the kinetics from experiment A,

175   removing 1% of the total gas from each domain, and then placing this gas in a new, highly diffusive domain with $\ln(\frac{D}{a^2})_1 = 23.4$, and $\phi_1 = 0.01$.

   To calculate the fractional releases and number of moles released after each heating step, we began with the equations for plane sheet geometry outlined in Ginster and Reiners (2018), which relate each heating step's duration, temperature, and the domain's $\ln(\frac{D_0}{a^2})_i$ to a fractional release from that domain $((F_{dom})_i)$. To determine the total gas fraction released for a sample

180   from each heating step (F_i), and not just for a specific domain $((F_{dom})_i)$, we summed the contributions from each domain as follows: $F_i = \sum_{i=1}^{n}(F_{dom})_i \phi_i$. In finding the number of moles released at each step, we calculated $M_i = F_i \cdot M_{tot}$, where

M_{tot} is the total number of atoms measured in Lovera et al.'s (1997) N13 K-feldspar experiment. To approximate uncertainties, we simply multiplied the percent error on the ^{40}Ar/^{39}Ar age from each step of the N13 experiment by M_i.

Using these synthetic degassing datasets, we attempted to solve for the prescribed diffusion kinetics of both experiments using our MDD Tool Kit optimization method (Lovera et al., 1997). Because K-feldspar is known to melt above 1100 °C (Luo et al., 2014), we excluded all calculated heating steps above 1100 °C in our misfit calculations.

5.2 Synthetic Data Results and Discussion

The MDD Tool Kit method successfully quantified the diffusion kinetics of both Experiment A and B, returning the correct E_a to within 0.02 kJ·mol^{-1} (Table 3, Figure 1). While the MDD Tool Kit routine did not perform as well in capturing ϕ_{6-8} in Experiment B, this is unsurprising since a higher percentage of the gas in those domains was released during the high-temperature steps excluded from the fitting exercise.

Lovera et al.'s (1997) algorithm correctly quantified the E_a of Experiment A, but it underestimated that of Experiment B by 9% (Table 3). While we did not implement a Levenberg-Marquardt method (Press, 2007) to solve for each $\ln(\frac{D_0}{a^2})_i$ and ϕ_i value, these parameters could not be correct given the incorrectly-predicted E_a.

Our synthetic experiment results clearly demonstrate that Lovera et al.'s (1997) algorithm can underestimate E_a (Figure 1). Any sample that contains at least one domain which loses a significant portion of its gas during initial heating steps is prone to this bias. Importantly, this error is not bi-directional; the Lovera algorithm will systematically underestimate E_a. In contrast, because the optimized E_a does not depend on a linear regression, but instead fits E_a as a free parameter, the MDD Tool Kit method appears to avoid this bias. This finding suggests that the use of the MDD Tool Kit to reanalyze any MDD-model-thermochronology study based on the Lovera approach would either produce similar results, or systematically higher temperatures through geologic time.

6 Case Study: Wong et al.'s (2023) Field Validation of the MDD Model

To assess the accuracy of the MDD model, Wong et al. (2023) conducted a field validation study of K-feldspar ^{40}Ar/^{39}Ar thermochronology at the Grayback normal fault block, AZ, USA. This field site is well studied, and several independent thermochronometers have been used here to measure geothermal gradients for application to models of continental extension (Howard and Foster, 1996; Wong et al., 2015).

The field validation primarily relies on four samples from various stratigraphic positions within the Tea Cup pluton, which intruded into the overlying $\sim$ 1.4 Ga Ruin Granite at $\sim$ 70 Ma (Banks et al., 1972). Samples originally from $\sim$ 12 km below the paleo-surface are accessible since these formations were tilted by $\sim$ 90° to the east during mid-Oligocene extension of the Greyback Fault (Banks et al., 1972; Wong et al., 2023). The straightforward stratigraphy and availability of independent thermochronometry data make this location optimal for the validation study.

Wong et al. (2023) found good agreement between their best-fitting ^{40}Ar/^{39}Ar t-T results and existing estimates of the paleo-geothermal gradient prior to mid-Oligocene extension (Howard and Foster, 1996; Wong et al., 2015, 2023). A secondary

assessment was provided by fission track, and (U-Th)/He ages in zircon and apatite. Although the observed ages generally do
215 not directly overlap in time with the K-feldspar MDD histories, the results do not preclude one another. In total, their study
appears to validate the MDD model. To determine whether the MDD Tool Kit method of fitting diffusion kinetics is consistent
with these independent observations, we reanalyze their ^{40}Ar/^{39}Ar stepwise degassing data using our new method.

6.1 Methods

6.1.1 Diffusion Kinetics

220 In determining the diffusion kinetics of each sample, Wong et al. (2023) used a modified version of Lovera et al.'s (1997)
fitting algorithm. Their primary modification was to fit an *unweighted* linear regression to the beginning heating steps from
each sample to determine E_a and $\ln \frac{D_0}{a_0^2}$. Instead of using the goodness-of-fit metric of Lovera et al. (1997), Wong et al. (2023),
varied how many heating steps they included in the regression, and explored the resultant effect of E_a on the constrained
t-T path. They note that adjusting the number of points in their regression, and therefore E_a, mainly affected the absolute
225 temperature predictions, and not the form of a t-T history. Although this was a routine choice given the tools available at
the time of their publication, such user-defined choices may introduce bias, a concern that the MDD Tool Kit inherently
circumvents.

In our application of the MDD Tool Kit to Wong et al.'s (2023) diffusion experiment results, we apply both the χ^2 and
$\%_{frac}$ misfit statistics defined above. As previously described, heating steps greater than 1100°C were excluded from our
230 misfit calculations.

6.1.2 Thermal Paths

When applying K-feldspar MDD modeling, a number of thermal histories are generated using a Monte Carlo-approach to
predict an ^{40}Ar/^{39}Ar age spectrum for each prescribed t-T path and using the sample's apparent diffusion kinetics. A misfit is
then calculated between the modeled and measured ^{40}Ar/^{39}Ar age spectra to determine the fitness of a particular t-T path.

235 In our study, we generated 30,000 thermal paths per sample and calculated radiogenic ^{40}Ar production and diffusive loss for
each t-T path using a Crank-Nicholson discretization of the diffusion equation for an infinite sheet geometry (Crank, 1975).
We then focus our analysis on the 100 best-fitting t-T paths for each sample based on the following misfit statistic:

$$\chi^2_{Age} = \frac{1}{N} \cdot \sum_{i=1}^{N} \left(\frac{(Age_{Measured})_i - (Age_{Modeled})_i}{(\sigma_{Age_{Measured}})_i} \right)^2 \tag{7}$$

where N is the number of steps included in the thermal modeling, and σ is the reported uncertainty on the final ^{40}Ar/^{39}Ar age.
240 As is common practice, Wong et al. (2023) ignored measurements thought to be contaminated with excess ^{40}Ar (^{40}Ar$_E$; Lovera
et al., 2002) for comparison with their results, we exclude the same data.

8

6.2 Results

Our predicted E_a values (Tables 4 – 6), regardless of misfit statistic, are systematically higher than those found by Wong et al. (2023) and are at the upper range of those published in Lovera et al.'s (1997) database of K-feldspar diffusion experiments. Given the bias inherent to the regression-fitting method (Figure 1), it is not surprising that our predicted E_a values are systematically higher, since the values of E_a were optimized using the entire dataset, rather than prescribed by linear regression to a subset of user-defined heating steps. And, although we defined a large search space for E_a, we find a smaller inter-sample range in predicted E_a than published by Wong et al. (2023), consistent with Lovera et al.'s (1997) observation that the variation of K-feldspar E_a values decreases when more gas is included in the E_a calculation.

Despite this finding, the choice of misfit statistic appears to influence the calculated diffusion kinetics of a given sample. In our analysis, choosing a χ^2 misfit instead of the $\%_{frac}$ misfit statistic led to intra-sample differences in the predicted E_a between 4.4 – 22.4 kJ·mol^{-1} (Tables 7 and 4, respectively). For example, there is a 22.4 kJ·mol^{-1} difference between the best-fit E_a value for sample GR-2 when using the χ^2 misfit compared to the $\%_{frac}$ misfit (Table 5). This disparity may provide an estimate of the uncertainty on the E_a, with the true E_a lying anywhere between those values.

An additional noteworthy model behavior emerged during our analysis. In three cases, the MDD Tool Kit identified at least one retentive domain that exhibited no gas diffusion throughout the simulated experiment, as indicated in Tables 4 – 7. The total ϕ value(s) of these domains typically equaled the gas quantity contained in the heating steps above 1100 °C. While the result that no gas diffused from the most retentive domain (or domains) during the simulated experiment may appear to suggest a poor model choice, this is not necessarily the case. Since K-feldspar begins to melt above 1100 °C, the MDD model is simply not applicable above this temperature. Furthermore, any domain retaining all its gas during simulation will yield identical release fractions, thereby making the model's fit insensitive to retentivities above a specific threshold (assuming all other parameters remain constant). Given our deliberate inclusion of a wide search space for each diffusion parameter and the stochastic nature of our optimization algorithm, such behavior is to be expected.

6.3 Reinterpretation of Field Calibration

Although our reinterpretation of these data largely finds t-T paths of similar form to those of Wong et al. (2023), our absolute temperature predictions are about 60 – 75 °C higher (Figure 4). To demonstrate that our approach yields results that are equally permissible, we compare them to the independent t-T constraints that exist at the Grayback fault.

Wong et al. (2023) proposed three criteria to assess the validity of an MDD model: (i) The thermal histories should be consistent with the stratigraphic heights of the samples, (ii) The form of the predictions should match prior work, including the timing, rate, and duration of cooling events, and (iii) The absolute temperatures should agree with those predicted by previous estimates of the pre-extensional geothermal gradient (Howard and Foster, 1996; Wong et al., 2015). The constrained t-T paths shown in Wong et al., (2023) and our re-analysis of the same dataset using the MDD Tool Kit both meet these criteria (Figure 4).

The predicted t-T paths for all four samples generally align with their respective stratigraphic positions; samples from higher
stratigraphic heights reflect the oldest portions of the thermal histories (Figure 4). Our findings reveal that the sample situated
at the highest stratigraphic level (GR-1) cooled below its Ar closure temperature around ~ 55 Ma, indicating relatively rapid
cooling between $\sim 70 - 55$ Ma. This trend is consistent with Howard and Foster's (1996) interpretation that the most shallow
depths of the pluton experienced rapid cooling as equilibrated with ambient temperatures.

MDD results for the next sample (GR-2), slightly deeper than GR-1, suggest a gradual cooling rate of approximately ~ 5
°C/Ma between $\sim 55 - 30$ Ma, consistent with the prediction of $\sim 4 - 6$ °C/Ma by Howard and Foster (1996).

The two samples at the lowest stratigraphic levels, GR-27 and GR-8, exhibit similar temperature histories. The median
pathway for GR-27 calculated with the χ^2 misfit indicates slightly higher temperatures compared to GR-8, despite the latter
occupying a slightly lower stratigraphic depth. However, given that their thermal pathways are within 1σ of each other, it
suggests that this technique may not be capable of resolving subtle differences between these samples. Moreover, the presence
of significant Ar_E (Lovera et al., 2002) in sample GR-8 introduces additional uncertainty into its Paleogene thermal history.
Despite the presence of Ar_E (Lovera et al., 2002), both of these deep stratigraphic samples demonstrate rapid cooling com-
mencing at around $\sim$ 27-28 Ma, consistent with the predicted timing of this cooling based on apatite fission track (AFT) ages
(Howard and Foster, 1996).

Finally, all four of our newly-calculated MDD models predict similar absolute temperatures to those estimated of the paleo-
geothermal gradient along the Tea Cup pluton prior to onset of extension along the Grayback fault. The paleo-gradient has been
estimated from temperature predictions made at 27 Ma at a variety of paleodepths using AFT (Howard and Foster, 1996). While
our estimates are consistently warmer than those calculated by Wong et al. (2023), they are still within the uncertainty bounds
of the predicted thermal gradient. The overall agreement between the rates and timing of cooling, as well as the relationship
between relative temperatures over time and the samples' stratigraphic order, indicates that the MDD Tool Kit generates t-T
results that are not excluded by the existing geologic and independent thermochronology data.

7   Conclusions

The Multiple Diffusion Domain model for $^{40}Ar/^{39}Ar$ thermochronology is valuable because it allows one to constrain a min-
eral's continuous thermal history through geologic time (McDougall and Harrison, 1999). However, the methods previously
used to empirically fit stepwise degassing data have required unverifiable assumptions about the grain size distribution of a
sample. Further, the commonly used method of quantifying E_a by fitting an uncertainty-weighted linear regression to the
lowest-temperature degassing steps of an experiment does not reliably return the correct values, but instead inadvertently in-
troduces a user bias. When this method fails to predict the correct value, it underestimates the true value. To address these
limitations, we present a new numerical routine that does not require fitting a linear regression to a user-defined subset of
heating steps to quantify a sample's E_a. Our new method utilizes a differential evolution algorithm to robustly search the
MDD-parameter space and solve for all parameters simultaneously. The code, entitled MDD Tool Kit, is open-source, pip-
installable, and available on GitHub. To evaluate its validity, we apply this new method to reinterpret the dataset published in

Wong et al.'s (2023) field validation of the ^{40}Ar/^{39}Ar K-feldspar MDD system at the Grayback fault. The diffusion kinetics fit by the MDD Tool Kit predict t-T paths that are consistent with independent observations and geologic constraints, and on average, 60 – 75 °C warmer than those previously published. We attribute this temperature difference to biases potentially introduced by the previously used modeling strategies.

Code availability. The code released in this publication is available at our github link: https://github.com/dgorin1/mddtoolkit

Appendix A: Supplemental Tables

For completeness, we include the optimization inputs used to reanalyze the experiments performed by Wong et al. (2023) (Tables A1–A4).

Author contributions. ALG and DLS conceived of the study. ALG and JMG designed the software. ALG, DLS, and MB contributed to the theory behind the software. ALG and DLS led manuscript writing. ALG constructed figures. All authors reviewed and edited the manuscript.

Competing interests. Authors declare that they have no competing interests.

References

Banks, N. G., Cornwall, H. R., Silberman, M. L., Creasey, S. C., and Marvin, R. F.: Chronology of Intrusion and Ore Deposition at Ray, Arizona; Part I, K-Ar Ages, Economic Geology, 67, 864–878, https://doi.org/10.2113/gsecongeo.67.7.864, 1972.

Crank, J.: The Mathematics of Diffusion, Oxford University Press, second edition edn., 1975.

325 Dodson, M. H.: Closure temperature in cooling geochronological and petrological systems, Contributions to Mineralogy and Petrology, 40, 259–274, https://doi.org/10.1007/BF00373790, 1973.

Fechtig, H. and Kalbitzer, S.: The Diffusion of Argon in Potassium-Bearing Solids, in: Potassium Argon Dating, pp. 68–107, Springer Berlin Heidelberg, Berlin, Heidelberg, https://doi.org/10.1007/978-3-642-87895-4_4, 1966.

Gillespie, A. R., Huneke, J. C., and Wasserburg, G. J.: An assessment of ^{40}Ar-^{39}Ar dating of incompletely degassed xenoliths, Journal of
330 Geophysical Research: Solid Earth, 87, 9247–9257, https://doi.org/10.1029/JB087iB11p09247, 1982.

Ginster, U. and Reiners, P. W.: Error Propagation in the Derivation of Noble Gas Diffusion Parameters for Minerals From Step Heating Experiments, Geochemistry, Geophysics, Geosystems, 19, 3706–3720, https://doi.org/10.1029/2018GC007531, 2018.

Grove, M., Lovera, O., and Harrison, M.: Late Cretaceous cooling of the east-central Peninsular Ranges Batholith (33 degrees N); relationship to La Posta Pluton emplacement, Laramide shallow subduction, and forearc sedimentation, in: Tectonic evolution of northwestern Mexico
335 and the Southwestern USA, Geological Society of America, https://doi.org/10.1130/0-8137-2374-4.355, 2003.

Harrison, T. M. and Lovera, O. M.: The multi-diffusion domain model: past, present and future, Geological Society, London, Special Publications, 378, 91–106, https://doi.org/10.1144/SP378.9, 2014.

Harrison, T. M., Copeland, P., Kidd, W. S. F., and Lovera, O. M.: Activation of the Nyainqentanghla Shear Zone: Implications for uplift of the southern Tibetan Plateau, Tectonics, 14, 658–676, https://doi.org/10.1029/95TC00608, 1995.

340 Howard, K. A. and Foster, D. A.: Thermal and unroofing history of a thick, tilted Basin-and-Range crustal section in the Tortilla Mountains, Arizona, Journal of Geophysical Research: Solid Earth, 101, 511–522, https://doi.org/10.1029/95JB02909, 1996.

Iman, R. L., Helton, J. C., and Campbell, J. E.: An Approach to Sensitivity Analysis of Computer Models: Part I—Introduction, Input Variable Selection and Preliminary Variable Assessment, Journal of Quality Technology, 13, 174–183, https://doi.org/10.1080/00224065.1981.11978748, 1981.

345 Lampinen, J.: A constraint handling approach for the differential evolution algorithm, in: Proceedings of the 2002 Congress on Evolutionary Computation. CEC'02 (Cat. No.02TH8600), vol. 2, pp. 1468–1473, IEEE, Honolulu, HI, USA, https://doi.org/10.1109/CEC.2002.1004459, 2002.

Lovera, O. M.: Computer programs to model 40Ar/39Ar diffusion data from multidomain samples, Computers & Geosciences, 18, 789–813, https://doi.org/10.1016/0098-3004(92)90025-M, 1992.

350 Lovera, O. M., Richter, F. M., and Harrison, T. M.: The ^{40}Ar/^{39}Ar thermochronometry for slowly cooled samples having a distribution of diffusion domain sizes, Journal of Geophysical Research: Solid Earth, 94, 17 917–17 935, https://doi.org/10.1029/JB094iB12p17917, 1989.

Lovera, O. M., Grove, M., Mark Harrison, T., and Mahon, K.: Systematic analysis of K-feldspar step heating results: I. Significance of activation energy determinations, Geochimica et Cosmochimica Acta, 61, 3171–3192, https://doi.org/10.1016/S0016-7037(97)00147-6,
355 1997.

Lovera, O. M., Grove, M., and Harrison, T.: Systematic analysis of K-feldspar 40 Ar/ 39 Ar step heating results II: relevance of laboratory argon diffusion properties to nature, Geochimica et Cosmochimica Acta, 66, 1237–1255, https://doi.org/10.1016/S0016-7037(01)00846-8, 2002.

Luo, G., Nie, X., Wu, S., and Wang, Y.: Influence of compound silicate gangue containing potassium in baiyunebo iron ore on solid-phase reactions during sintering process, in: Recent Advances in Structural Integrity Analysis - Proceedings of the International Congress (APCF/SIF-2014), pp. 473–476, Elsevier, https://doi.org/10.1533/9780081002254.473, 2014.

McDougall, I. and Harrison, T. M.: Geochronology and Thermochronology by the 40Ar/39Ar Method, Oxford University Press, 1999.

Parsons, I., Brown, W. L., and Smith, J. V.: 40 Ar/ 39 Ar thermochronology using alkali feldspars: real thermal history or mathematical mirage of microtexture?, Contributions to Mineralogy and Petrology, 136, 92–110, https://doi.org/10.1007/s004100050526, 1999.

Press, W. H., ed.: Numerical recipes: the art of scientific computing, Cambridge University Press, Cambridge, UK ; New York, 3rd ed edn., oCLC: ocn123285342, 2007.

Qiang, J. and Mitchell, C.: A Unified Differential Evolution Algorithm for Global Optimization, https://www.osti.gov/servlets/purl/1163659, 2014.

Quidelleur, X., Grove, M., Lovera, O. M., Harrison, T. M., Yin, A., and Ryerson, F. J.: Thermal evolution and slip history of the Renbu Zedong Thrust, southeastern Tibet, Journal of Geophysical Research: Solid Earth, 102, 2659–2679, https://doi.org/10.1029/96JB02483, 1997.

Reiners, P. W.: Past, Present, and Future of Thermochronology, Reviews in Mineralogy and Geochemistry, 58, 1–18, https://doi.org/10.2138/rmg.2005.58.1, 2005.

Reiners, P. W., Carlson, R. W., Renne, P. R., Cooper, K. M., Granger, D. E., McLean, N. M., and Schoene, B.: Geochronology and thermochronology, John Wiley & Sons, 2017.

Shuster, D. L., Farley, K. A., Sisterson, J. M., and Burnett, D. S.: Quantifying the diffusion kinetics and spatial distributions of radiogenic 4He in minerals containing proton-induced 3He, Earth and Planetary Science Letters, 217, 19–32, https://doi.org/10.1016/S0012-821X(03)00594-6, 2004.

Storn, R. and Price, K.: Differential Evolution – A simple and Efficient Heuristic for Global Optimization over Continuous Spaces, Journal of Global Optimization, 11, 341–359, https://doi.org/10.1023/A:1008202821328, 1997.

Turner, G.: The Distribution of Potassium and Argon in Chondrites, in: Origin and Distribution of the Elements, pp. 387–398, Elsevier, https://doi.org/10.1016/B978-0-08-012835-1.50039-8, 1968.

Villa, I. M.: Multipath Ar transport in K-feldspar deduced from isothermal heating experiments, Earth and Planetary Science Letters, 122, 393–401, https://doi.org/10.1016/0012-821X(94)90010-8, 1994.

Virtanen, P., Gommers, R., Oliphant, T. E., Haberland, M., Reddy, T., Cournapeau, D., Burovski, E., Peterson, P., Weckesser, W., Bright, J., Van Der Walt, S. J., Brett, M., Wilson, J., Millman, K. J., Mayorov, N., Nelson, A. R. J., Jones, E., Kern, R., Larson, E., Carey, C. J., Polat, , Feng, Y., Moore, E. W., VanderPlas, J., Laxalde, D., Perktold, J., Cimrman, R., Henriksen, I., Quintero, E. A., Harris, C. R., Archibald, A. M., Ribeiro, A. H., Pedregosa, F., Van Mulbregt, P., SciPy 1.0 Contributors, Vijaykumar, A., Bardelli, A. P., Rothberg, A., Hilboll, A., Kloeckner, A., Scopatz, A., Lee, A., Rokem, A., Woods, C. N., Fulton, C., Masson, C., Häggström, C., Fitzgerald, C., Nicholson, D. A., Hagen, D. R., Pasechnik, D. V., Olivetti, E., Martin, E., Wieser, E., Silva, F., Lenders, F., Wilhelm, F., Young, G., Price, G. A., Ingold, G.-L., Allen, G. E., Lee, G. R., Audren, H., Probst, I., Dietrich, J. P., Silterra, J., Webber, J. T., Slavič, J., Nothman, J., Buchner, J., Kulick, J., Schönberger, J. L., De Miranda Cardoso, J. V., Reimer, J., Harrington, J., Rodríguez, J. L. C., Nunez-Iglesias, J., Kuczynski, J., Tritz, K., Thoma, M., Newville, M., Kümmerer, M., Bolingbroke, M., Tartre, M., Pak, M., Smith, N. J., Nowaczyk, N., Shebanov, N.,

Pavlyk, O., Brodtkorb, P. A., Lee, P., McGibbon, R. T., Feldbauer, R., Lewis, S., Tygier, S., Sievert, S., Vigna, S., Peterson, S., More,

395   S., Pudlik, T., Oshima, T., Pingel, T. J., Robitaille, T. P., Spura, T., Jones, T. R., Cera, T., Leslie, T., Zito, T., Krauss, T., Upadhyay, U.,
      Halchenko, Y. O., and Vázquez-Baeza, Y.: SciPy 1.0: fundamental algorithms for scientific computing in Python, Nature Methods, 17,
      261–272, https://doi.org/10.1038/s41592-019-0686-2, 2020.

Wagner, A.: Cooling ages derived by apatite fission-track, mica Rb-Sr and K-Ar dating ; the uplift and cooling history of the Central Alps,
      Mem. Inst. Geol. Mineral., Univ. of Padova, 30, 1–27, https://cir.nii.ac.jp/crid/1570854175293805312, 1977.

400   Weirich, J., Isachsen, C., Johnson, J., and Swindle, T.: Variability of diffusion of argon in albite, pyroxene, and olivine in shocked and
      unshocked samples, Geochimica et Cosmochimica Acta, 77, 546–560, https://doi.org/10.1016/j.gca.2011.10.040, 2012.

Wong, M. S., Gleason, D. M., O'Brien, H. P., and Idleman, B. D.: Confirmation of a low pre-extensional geothermal gradient in the Grayback
      normal fault block, Arizona: Structural and AHe thermochronologic evidence, Geological Society of America Bulletin, 127, 200–210,
      https://doi.org/10.1130/B31033.1, 2015.

405   Wong, M. S., Gans, P. B., and Roesler, D.: Field calibration of 40Ar/39Ar K-feldspar multiple diffusion domain (MDD) thermal histories at
      the Grayback normal fault block, Arizona, USA, Geology, 51, 885–889, https://doi.org/10.1130/G51319.1, 2023.

Zeitler, P. K.: Argon diffusion in partially outgassed alkali feldspars: Insights from analysis, Chemical Geology: Isotope Geoscience section,
      65, 167–181, https://doi.org/10.1016/0168-9622(87)90071-6, 1987.
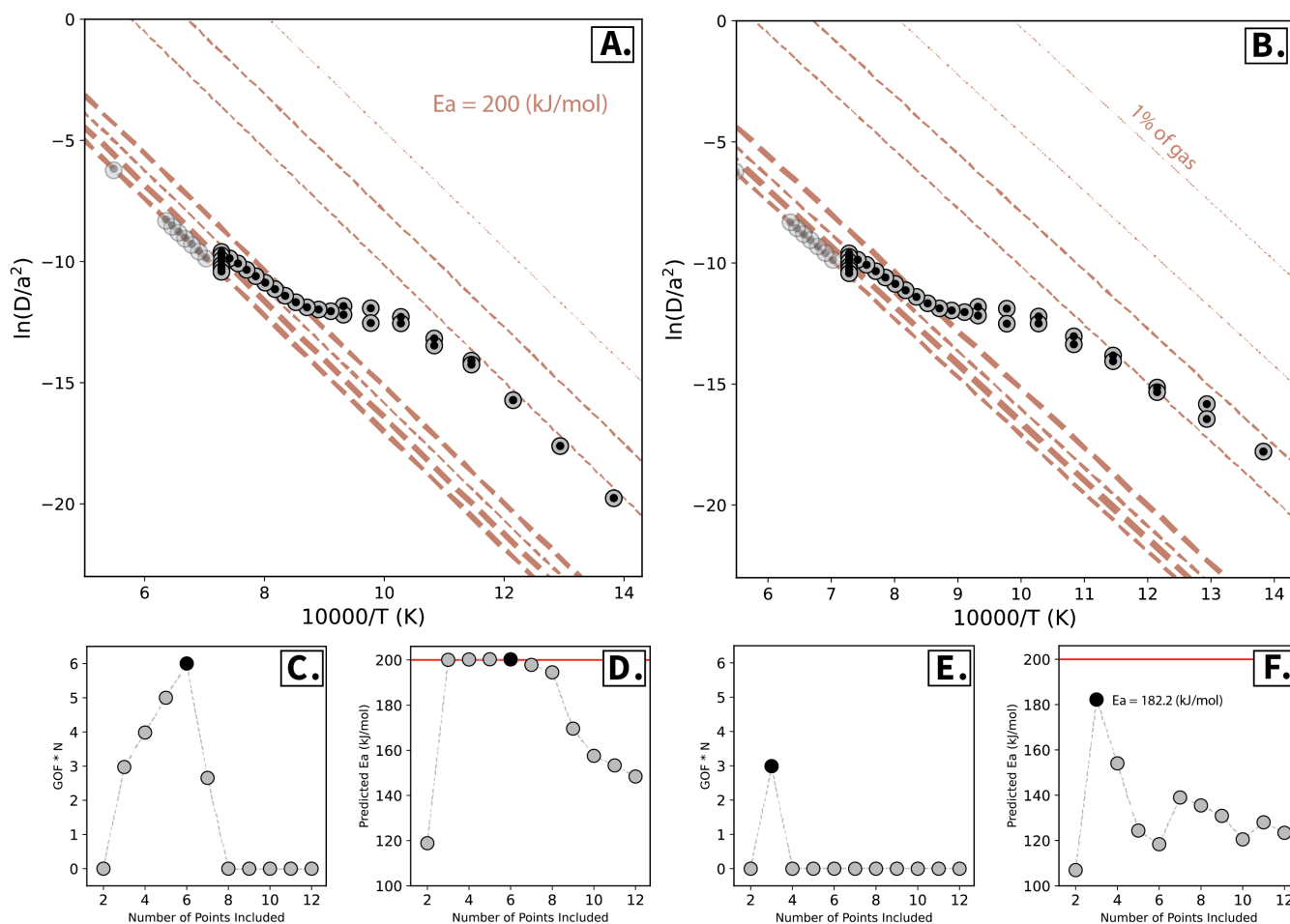
Figure 1. A. Arrhenius plot resulting from synthetic Experiment A. Gray Circles show the expected $\frac{D}{a^2}$ values calculated from the pre-determined diffusion kinetics (Table 3), and transparent gray circles show the heating steps excluded from the fitting exercise. Black circles represent the values predicted by the MDD Tool Kit method. **B.** Same as A. except showing the expected $\frac{D}{a^2}$ values calculated from the pre-determined diffusion kinetics for Experiment B. **C.** Value of $q \cdot N$ as the number of points included in the uncertainty-weighted linear regression increases for Experiment A. Lovera et al.'s (1997) algorithm for determining the E_a maximizes the value of this function to determine the appropriate number of points to include. The black dot indicates this value. **D.** The predicted E_a as one increases the number of points included in the unweighted linear regression. The black point indicates the E_a selected by Lovera et al.'s (1997) algorithm for Experiment A. In this case, the algorithm selects the correct E_a. E. Same as panel C, but showing the results for synthetic Experiment B. **F.** Same as panel D but for synthetic Experiment B. In this case, Lovera et al.'s (1997) algorithm underestimates the correct E_a.
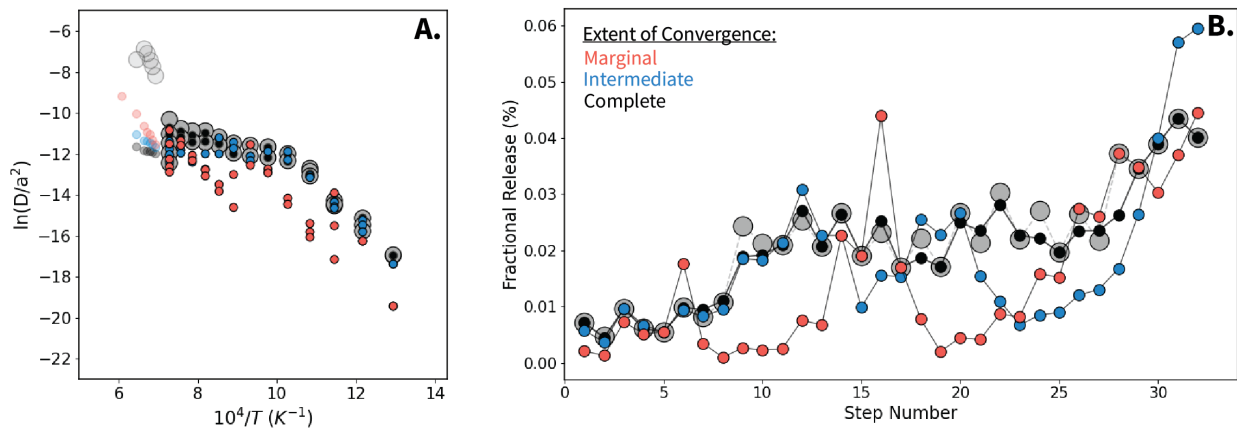
Figure 2. A. Results of an MDD Tool Kit optimization applied to Wong et al.'s (2023) sample GR-27 demonstrating the iterative nature of the improvement using the $\%_{frac}$ misfit statistic shown in Arrhenius space. **B.** Same as A, but shown in the space where the optimization is performed–the fractional release at each heating step. Red circles show the optimization halted after 8 iterations ($\%_{frac} = 15.06$), blue circles show the same optimization halted after 28 iterations ($\%_{frac} = 8.33$), and black circles show the same optimization results after complete convergence after 18,419 iterations ($\%_{frac} = 1.82$). The gray circles show the observed results.
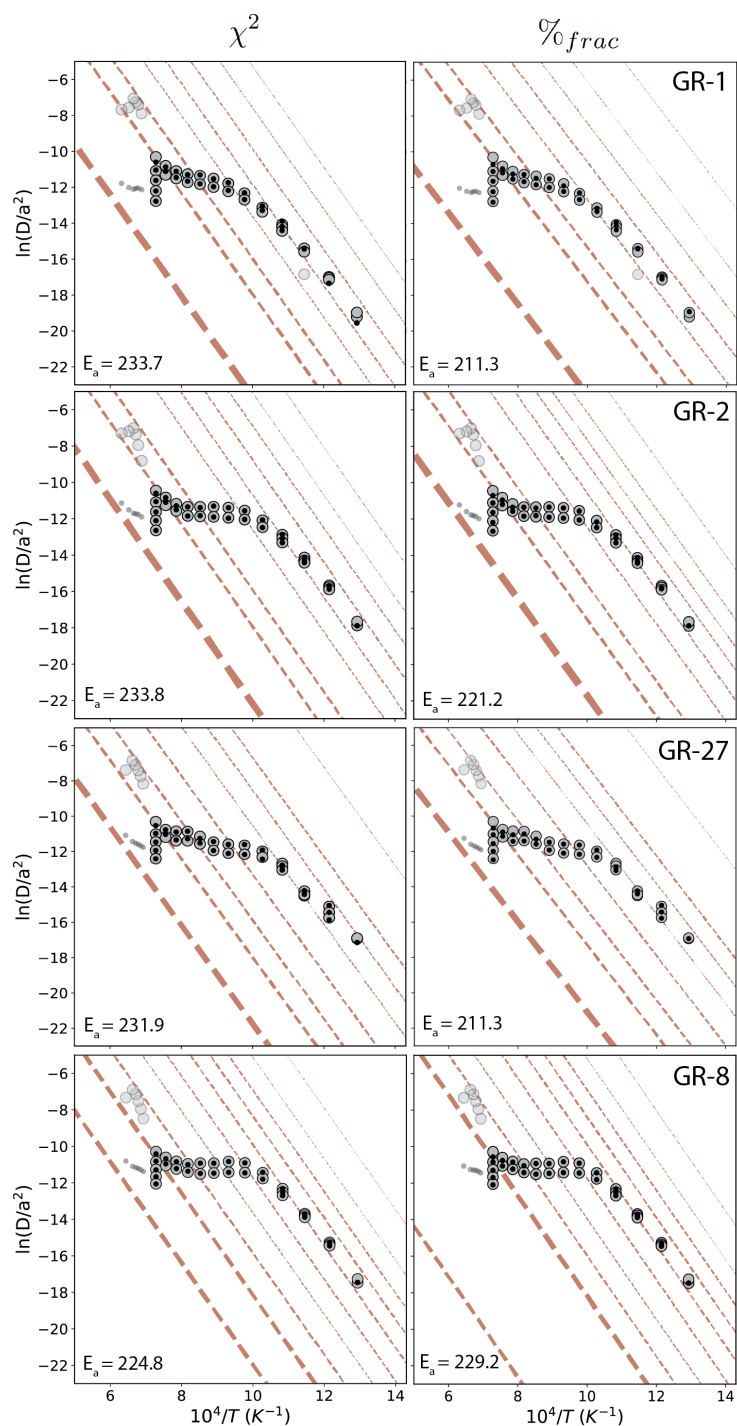
Figure 3. Arrhenius plots showing our reanalysis of Wong et al.'s (2023) samples with both the χ^2 and $\%_{frac}$ misfit statistics. Red lines represent the diffusion kinetics of each individual domain, and their thicknesses are proportional to domain's ϕ value. Gray circles show the experimental results and black dots show the MDD model predictions. All E_a are given in kJ·mol^{-1}
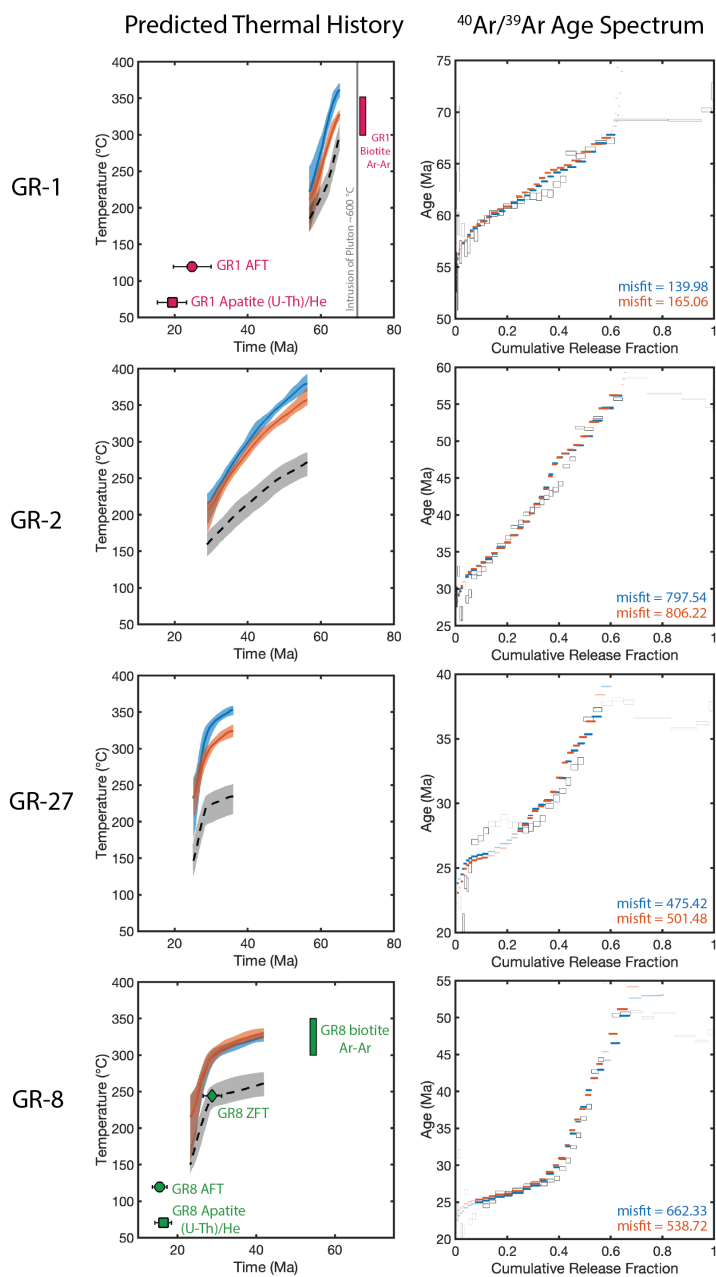
Figure 4. Resulting best-fit thermal pathways and ^{40}Ar-^{39}Ar age spectra from our reanalysis of Wong et al.'s (2023) field validation of the MDD method in K-feldspar. Blue shaded regions in the thermal history plots correspond to the χ^2 misfit statistic. The orange shaded regions correspond to the $\%_{frac}$ misfit statistic. More specifically, the shaded regions represent a 1σ deviation from the median of the top 100 best-fitting thermal paths for a given sample (plotted in bold). The dotted line and gray regions represent Wong et al.'s (2023) predictions for the same samples. The ^{40}Ar/^{39}Ar age spectrum plots show the predicted ^{40}Ar/^{39}Ar Ages for the median χ^2 (blue) and $\%_{frac}$ (orange) thermal paths. Grey boxes represent the measured values from Wong (2023). Heating steps excluded from the modeling exercise are made to be transparent.
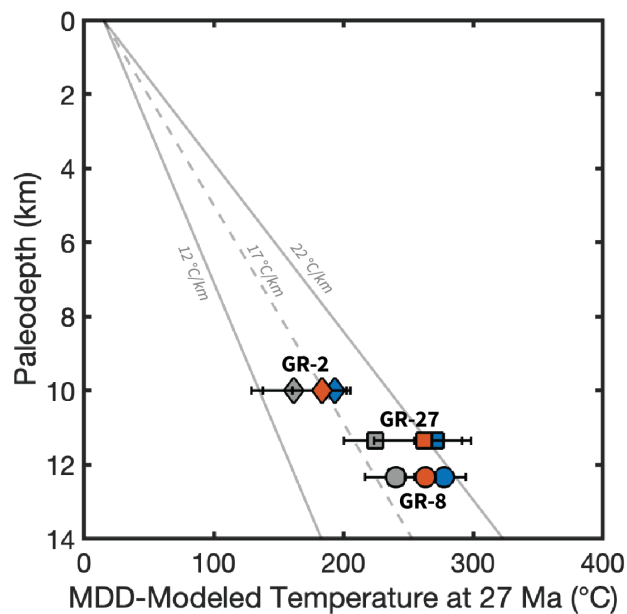
Figure 5. Predicted paleotemperatures at 27 Ma from samples GR-2, GR-27, and GR-8. The gray symbols represent Wong et al.'s (2023) results, the orange symbols represent our results from the $\%_{frac}$ misfit statistic, and the blue symbols represent our results from the χ^2 misfit statistic.

Table 1. Equations used by the MDD Tool Kit to calculate f, the fractional loss from each domain during each heating step in a stepwise degassing experiment (Crank, 1975; Ginster and Reiners, 2018).

Geometry	Equation	Validity
Sphere (radius a)	$f = 1 - \frac{6}{\pi^2}\sum_1^\infty \frac{1}{n^2}\exp(\frac{-n^2\pi^2 Dt}{a^2})$	All f
	$f \approx 1 - \frac{6}{\pi^2}\exp(\frac{-\pi^2 Dt}{a^2})$	$0.85 \leq f \leq= 1$
	$f \approx \frac{6}{\pi^{\frac{3}{2}}}\sqrt{\frac{\pi^2 Dt}{a^2}} - \frac{3Dt}{a^2}$	$0 \leq f \leq 0.85$
Plane Sheet (half-width a	$f = 1 - \frac{8}{\pi^2}\sum_1^\infty \frac{1}{(2n+1)^2}\exp[-(2n+1)^2\pi^2\frac{Dt}{4a^2}]$	All f
	$f \approx 1 - \frac{8}{\pi^2}\exp(\frac{\pi^2 Dt}{4a^2})$	$0.45 \leq f \leq 1$
	$f \approx \frac{2}{\sqrt{\pi}}\sqrt{\frac{Dt}{a^2}}$	$0 \leq f \leq 0.60$

Table 2. Parameter search ranges used in this publication. These values can be adjusted in the open-access code.

Parameter	Search Range
$\hat{M}_{tot}$ (Moles)	$(\hat{M}_{tot} - 3\sigma, \hat{M}_{tot} + 3\sigma)$
E_a (kJ/mol)	(50, 500)
$\ln\left(\frac{D_0}{a^2}\right) (s^{-1})$	(-5, 50)
ϕ (normalized units)	(0, 1)

Table 3. Setup and results of synthetic diffusion experiment optimizations. Experiment A and B are the same except that a domain with $\ln(\frac{D_0}{a^2})_1$ has been added to experiment B. To redistribute the gas, 1% was removed from all other domains such that $\phi_1 = 0.01$.

	Experiment A	Optimization Results A	Experiment B	Optimization Results B
M_{tot} ($\cdot 10^{-12}$)	5.21	5.21	5.21	5.21
E_a ($\frac{kJ}{mol}$)	200.2	200.0	200.2	200.3
$\ln(\frac{D_0}{a^2})_1$	19.45	19.42	23.8	23.81
$\ln(\frac{D_0}{a^2})_2$	16.18	16.14	19.45	19.46
$\ln(\frac{D_0}{a^2})_3$	13.93	13.90	16.18	16.19
$\ln(\frac{D_0}{a^2})_4$	8.89	8.88	13.93	13.94
$\ln(\frac{D_0}{a^2})_5$	8.09	8.18	8.89	8.89
$\ln(\frac{D_0}{a^2})_6$	7.51	7.58	8.09	8.04
$\ln(\frac{D_0}{a^2})_7$	6.98	7.02	7.51	7.49
$\ln(\frac{D_0}{a^2})_8$	–	–	6.98	6.97
ϕ_1	0.025	0.025	0.01	0.01
ϕ_2	0.097	0.097	0.025	0.025
ϕ_3	0.082	0.082	0.096	0.096
ϕ_4	0.226	0.214	0.082	0.082
ϕ_5	0.127	0.109	0.224	0.233
ϕ_6	0.273	0.252	0.125	0.129
ϕ_7	0.170	0.220	0.270	0.266
ϕ_8	–	–	0.168	0.160

Table 4. Results from sample GR-1.

Sample GR-1 Diffusion Kinetics	Wong (2023) Results	χ^2 (This Work)	$\%_{frac}$ (This Work)
E_a ($\frac{kJ}{mol}$)	187.1	233.7	211.3
$\ln(\frac{D_0}{a^2})_1$	14.63	22.8	23.1
$\ln(\frac{D_0}{a^2})_2$	12.57	20.5	19.3
$\ln(\frac{D_0}{a^2})_3$	10.75	18.3	17.0
$\ln(\frac{D_0}{a^2})_4$	7.85	16.3	14.8
$\ln(\frac{D_0}{a^2})_5$	7.76	14.50	12.8
$\ln(\frac{D_0}{a^2})_6$	6.05	12.1	10.1
$\ln(\frac{D_0}{a^2})_7$	3.77	10.2	8.2
$\ln(\frac{D_0}{a^2})_8$	1.14	4.4	1.9
ϕ_1	0.049	0.022	0.001
ϕ_2	0.088	0.044	0.026
ϕ_3	0.094	0.073	0.056
ϕ_4	0.111	0.080	0.090
ϕ_5	0.096	0.058	0.085
ϕ_6	0.127	0.145	0.148
ϕ_7	0.101	0.187	0.196
ϕ_8	0.033	0.391	0.398

Table 5. Results from sample GR-2.

Sample GR-2 Diffusion Kinetics	Wong (2023) Results	χ^2 (This Work)	$\%_{frac}$
$E_a\ (\frac{kJ}{mol})$	182.0	233.8	221.2
$\ln(\frac{D_0}{a^2})_1$	17.36	25.7	23.2
$\ln(\frac{D_0}{a^2})_2$	15.43	23.0	20.5
$\ln(\frac{D_0}{a^2})_3$	13.65	21.2	18.9
$\ln(\frac{D_0}{a^2})_4$	11.76	19.4	17.7
$\ln(\frac{D_0}{a^2})_5$	8.49	17.4	16.0
$\ln(\frac{D_0}{a^2})_6$	8.46	15.5	14.2
$\ln(\frac{D_0}{a^2})_6$	6.53	12.2	11.0
$\ln(\frac{D_0}{a^2})_8$	4.44	10.2	9.1
$\ln(\frac{D_0}{a^2})_9$	1.79	5.9	4.9
ϕ_1	0.036	0.009	0.011
ϕ_2	0.092	0.022	0.045
ϕ_3	0.096	0.066	0.052
ϕ_4	0.074	0.081	0.067
ϕ_5	0.05	0.074	0.072
ϕ_6	0.119	0.064	0.069
ϕ_7	0.145	0.134	0.121
ϕ_8	0.076	0.157	0.154
ϕ_9	0.312	0.393	0.410

Table 6. Results from sample GR-27.

Sample GR-27 Diffusion Kinetics	Wong (2023) Results	χ^2 (This Work)	Percent_Frac (This Work)
$E_a \left(\frac{kJ}{mol} \right)$	159.5	231.9	211.3
$\ln \left(\frac{D_0}{a^2} \right)_1$	11.2	26.3	23.3
$\ln \left(\frac{D_0}{a^2} \right)_2$	9.9	21.2	18.2
$\ln \left(\frac{D_0}{a^2} \right)_3$	7.5	19.4	16.7
$\ln \left(\frac{D_0}{a^2} \right)_4$	5.2	17.4	15.0
$\ln \left(\frac{D_0}{a^2} \right)_5$	5.0	14.6	12.6
$\ln \left(\frac{D_0}{a^2} \right)_6$	2.9	12.0	10.1
$\ln \left(\frac{D_0}{a^2} \right)_6$	2.0	9.9	8.1
$\ln \left(\frac{D_0}{a^2} \right)_8$	-0.1	6.1	4.3
ϕ_1	0.124	0.015	0.013
ϕ_2	0.064	0.092	0.098
ϕ_3	0.109	0.077	0.070
ϕ_4	0.117	0.053	0.050
ϕ_5	0.102	0.114	0.103
ϕ_6	0.104	0.130	0.121
ϕ_7	0.112	0.171	0.168
ϕ_8	0.268	0.348	0.377

Table 7. Results from sample GR-8.

Sample GR-8 Diffusion Kinetics	Wong (2023) Results	χ^2 (This Work)	$\%_{frac}$
$E_a\ (\frac{kJ}{mol})$	182.0	224.8	229.2
$\ln(\frac{D_0}{a^2})_1$	14.9	24.2	25.0
$\ln(\frac{D_0}{a^2})_2$	13.5	21.1	21.9
$\ln(\frac{D_0}{a^2})_3$	11.9	19.3	19.8
$\ln(\frac{D_0}{a^2})_4$	10.2	17.5	17.8
$\ln(\frac{D_0}{a^2})_5$	7.5	15.6	15.9
$\ln(\frac{D_0}{a^2})_6$	7.5	13.7	13.6
$\ln(\frac{D_0}{a^2})_6$	5.5	11.4	11.8
$\ln(\frac{D_0}{a^2})_8$	4.3	9.0	10.0
$\ln(\frac{D_0}{a^2})_9$	2.7	-4.1	7.5
ϕ_1	0.053	0.009	0.008
ϕ_2	0.152	0.048	0.050
ϕ_3	0.111	0.125	0.136
ϕ_4	0.080	0.109	0.106
ϕ_5	0.075	0.082	0.085
ϕ_6	0.074	0.058	0.062
ϕ_7	0.143	0.118	0.081
ϕ_8	0.061	0.260	0.107
ϕ_9	0.252	0.191	0.365

Table A1. Sample GR-1 input (Wong et al., 2023).

Step Number	Temperature (°C)	Duration (Hours)	^{39}Ar Released (Moles)	Measurement Uncertainty (Moles; 1-σ)	Included in Diffusion Kinetics Optimization? (1=yes, 2=no)
0	500	0.250	2.54E-16	8.40E-19	1
1	500	0.417	1.95E-16	7.58E-19	1
2	550	0.250	4.44E-16	1.22E-18	1
3	550	0.333	3.50E-16	1.05E-18	1
4	550	0.500	3.58E-16	8.48E-19	1
5	600	0.250	7.40E-16	1.29E-18	1
6	600	0.333	1.89E-16	7.23E-19	0
7	600	0.500	8.21E-16	1.57E-18	1
8	650	0.250	1.37E-15	1.87E-18	1
9	650	0.333	1.19E-15	1.59E-18	1
10	650	0.500	1.18E-15	1.43E-18	1
11	700	0.250	1.77E-15	2.23E-18	1
12	700	0.333	1.54E-15	1.75E-18	1
13	750	0.250	2.68E-15	2.59E-18	1
14	750	0.333	2.06E-15	2.29E-18	1
15	800	0.250	3.24E-15	2.84E-18	1
16	800	0.333	2.37E-15	2.58E-18	1
17	850	0.250	3.19E-15	2.79E-18	1
18	850	0.333	2.34E-15	2.40E-18	1
19	900	0.250	2.99E-15	3.27E-18	1
20	900	0.333	2.27E-15	2.22E-18	1
21	950	0.250	2.76E-15	2.62E-18	1
22	950	0.333	2.17E-15	2.14E-18	1

410

Step Number	Temperature (°C)	Duration (Hours)	^{39}Ar Released (Moles)	Measurement Uncertainty (Moles; 1-σ)	Included in Diffusion Kinetics Optimization? (1=yes, 2=no)
23	1000	0.250	2.86E-15	2.47E-18	1
24	1000	0.333	2.34E-15	2.47E-18	1
25	1050	0.250	3.34E-15	3.08E-18	1
26	1050	0.333	2.51E-15	2.30E-18	1
27	1100	0.250	4.76E-15	3.70E-18	1
28	1100	0.500	4.01E-15	3.26E-18	1
29	1100	1.000	4.41E-15	2.98E-18	1
30	1100	2.000	4.54E-15	3.74E-18	1
31	1100	3.333	3.73E-15	7.08E-18	1
32	1180	0.233	2.29E-14	8.27E-18	0
33	1200	0.233	1.41E-14	7.50E-18	0
34	1215	0.233	4.24E-15	3.30E-18	0
35	1230	0.233	1.07E-15	1.46E-18	0
36	1260	0.233	1.44E-16	6.39E-19	0
37	1310	0.233	4.61E-17	4.30E-19	0
38	1370	0.233	2.87E-17	3.34E-19	0

Table A2. Sample GR-2 input (Wong et al., 2023).

Step Number	Temperature (°C)	Duration (Hours)	^{39}Ar Released (Moles)	Measurement Uncertainty (Moles; 1-σ)	Included in Diffusion Kinetics Optimization? (1=yes, 2=no)
0	500	0.250	6.43E-16	1.22E-18	1
1	500	0.417	4.82E-16	1.09E-18	1
2	550	0.250	1.11E-15	1.62E-18	1
3	550	0.333	8.51E-16	1.41E-18	1
4	550	0.500	8.55E-16	1.47E-18	1
5	600	0.250	1.79E-15	2.02E-18	1
6	600	0.333	1.51E-15	1.79E-18	1
7	600	0.500	1.62E-15	2.12E-18	1
8	650	0.250	2.94E-15	2.47E-18	1
9	650	0.333	2.59E-15	2.83E-18	1
10	650	0.500	2.54E-15	2.81E-18	1
11	700	0.250	3.58E-15	2.98E-18	1
12	700	0.333	2.80E-15	2.49E-18	1
13	750	0.250	4.49E-15	3.20E-18	1
14	750	0.333	3.17E-15	2.08E-18	1
15	800	0.250	4.10E-15	2.59E-18	1
16	800	0.333	2.83E-15	2.30E-18	1
17	850	0.250	3.57E-15	3.04E-18	1
18	850	0.333	2.54E-15	2.42E-18	1
19	900	0.250	3.09E-15	2.67E-18	1
20	900	0.333	2.30E-15	2.23E-18	1
21	950	0.250	2.77E-15	2.38E-18	1
22	950	0.333	2.15E-15	2.61E-18	1

Step Number	Temperature (°C)	Duration (Hours)	^{39}Ar Released (Moles)	Measurement Uncertainty (Moles; 1-σ)	Included in Diffusion Kinetics Optimization? (1=yes, 2=no)
23	1000	0.250	2.99E-15	2.92E-18	1
24	1000	0.333	2.57E-15	2.73E-18	1
25	1050	0.250	3.82E-15	3.57E-18	1
26	1050	0.333	3.15E-15	3.13E-18	1
27	1100	0.250	4.97E-15	3.45E-18	1
28	1100	0.500	4.89E-15	3.55E-18	1
29	1100	1.000	5.39E-15	3.80E-18	1
30	1100	2.000	5.82E-15	3.99E-18	1
31	1100	3.333	5.15E-15	3.53E-18	1
32	1180	0.233	1.36E-14	5.42E-18	0
33	1200	0.233	1.95E-14	6.50E-18	0
34	1215	0.233	1.32E-14	5.65E-18	0
35	1230	0.233	4.09E-15	3.01E-18	0
36	1260	0.233	5.86E-16	1.14E-18	0
37	1310	0.233	1.16E-16	5.24E-19	0
38	1370	0.233	3.83E-17	2.94E-19	0

Table A3. Sample GR-8 input (Wong et al., 2023).

Step Number	Temperature (°C)	Duration (Hours)	^{39}Ar Released (Moles)	Measurement Uncertainty (Moles; 1-σ)	Included in Diffusion Kinetics Optimization? (1=yes, 2=no)
0	500	0.250	8.31E-16	1.64E-18	1
1	500	0.417	6.20E-16	1.28E-18	1
2	550	0.250	1.45E-15	1.90E-18	1
3	550	0.333	1.11E-15	1.64E-18	1
4	550	0.500	1.15E-15	1.51E-18	1
5	600	0.250	2.39E-15	2.21E-18	1
6	600	0.333	2.15E-15	2.20E-18	1
7	600	0.500	2.30E-15	2.62E-18	1
8	650	0.250	4.23E-15	3.29E-18	1
9	650	0.333	3.66E-15	3.21E-18	1
10	650	0.500	3.81E-15	3.02E-18	1
11	700	0.250	5.43E-15	3.41E-18	1
12	700	0.333	4.46E-15	3.56E-18	1
13	750	0.250	6.65E-15	2.86E-18	1
14	750	0.333	4.52E-15	4.01E-18	1
15	800	0.250	5.59E-15	3.13E-18	1
16	800	0.333	3.76E-15	2.88E-18	1
17	850	0.250	4.29E-15	2.93E-18	1
18	850	0.333	3.13E-15	2.72E-18	1
19	900	0.250	3.82E-15	3.08E-18	1
20	900	0.333	2.68E-15	3.01E-18	1
21	950	0.250	3.35E-15	2.68E-18	1
22	950	0.333	2.71E-15	2.66E-18	1

Step Number	Temperature (°C)	Duration (Hours)	^{39}Ar Released (Moles)	Measurement Uncertainty (Moles; 1-σ)	Included in Diffusion Kinetics Optimization? (1=yes, 2=no)
23	1000	0.250	3.54E-15	3.49E-18	1
24	1000	0.333	2.96E-15	2.67E-18	1
25	1050	0.250	4.02E-15	3.14E-18	1
26	1050	0.333	3.29E-15	2.90E-18	1
27	1100	0.250	4.75E-15	3.75E-18	1
28	1100	0.500	5.01E-15	2.75E-18	1
29	1100	1.000	5.95E-15	3.19E-18	1
30	1100	2.000	7.04E-15	3.86E-18	1
31	1100	3.333	6.73E-15	3.29E-18	1
32	1170	0.233	1.25E-14	5.57E-18	0
33	1185	0.233	1.20E-14	6.19E-18	0
34	1200	0.233	7.56E-15	4.37E-18	0
35	1215	0.233	2.91E-15	2.59E-18	0
36	1235	0.233	6.00E-16	1.31E-18	0
37	1280	0.233	6.11E-17	3.71E-19	0
38	1370	0.233	2.11E-17	2.49E-19	0

Table A4. Sample GR-27 input (Wong et al., 2023).

Step Number	Temperature (°C)	Duration (Hours)	^{39}Ar Released (Moles)	Measurement Uncertainty (Moles; 1-σ)	Included in Diffusion Kinetics Optimization? (1=yes, 2=no)
0	500	0.250	1.23E-15	2.19E-18	1
1	500	0.417	8.07E-16	1.55E-18	1
2	550	0.250	1.66E-15	2.25E-18	1
3	550	0.333	1.07E-15	1.56E-18	1
4	550	0.500	9.55E-16	1.46E-18	1
5	600	0.250	1.72E-15	1.91E-18	1
6	600	0.333	1.41E-15	1.92E-18	1
7	600	0.500	1.87E-15	1.86E-18	1
8	650	0.250	4.23E-15	3.52E-18	1
9	650	0.333	3.69E-15	2.82E-18	1
10	650	0.500	3.65E-15	3.31E-18	1
11	700	0.250	4.40E-15	3.73E-18	1
12	700	0.333	3.60E-15	2.76E-18	1
13	750	0.250	4.62E-15	3.53E-18	1
14	750	0.333	3.32E-15	2.79E-18	1
15	800	0.250	4.02E-15	3.26E-18	1
16	800	0.333	2.94E-15	2.38E-18	1
17	850	0.250	3.85E-15	2.81E-18	1
18	850	0.333	2.96E-15	2.35E-18	1
19	900	0.250	4.62E-15	3.34E-18	1
20	900	0.333	3.71E-15	2.78E-18	1
21	950	0.250	5.26E-15	3.46E-18	1
22	950	0.333	3.82E-15	4.29E-18	1

415

Step Number	Temperature (°C)	Duration (Hours)	^{39}Ar Released (Moles)	Measurement Uncertainty (Moles; 1-σ)	Included in Diffusion Kinetics Optimization? (1=yes, 2=no)
23	1000	0.250	4.68E-15	2.43E-18	1
24	1000	0.333	3.41E-15	2.96E-18	1
25	1050	0.250	4.61E-15	3.73E-18	1
26	1050	0.333	3.78E-15	3.05E-18	1
27	1100	0.250	6.47E-15	4.04E-18	1
28	1100	0.500	5.98E-15	3.31E-18	1
29	1100	1.000	6.76E-15	3.86E-18	1
30	1100	2.000	7.55E-15	4.27E-18	1
31	1100	3.333	6.95E-15	4.17E-18	1
32	1170	0.233	2.40E-14	9.26E-18	0
33	1185	0.233	1.78E-14	6.38E-18	0
34	1200	0.233	8.52E-15	5.10E-18	0
35	1215	0.233	2.82E-15	2.87E-18	0
36	1235	0.233	5.46E-16	1.04E-18	0
37	1280	0.233	4.93E-17	4.16E-19	0
38	1370	0.233	1.88E-17	2.55E-19	0